Subject-specific maximum entropy model of resting state fMRI shows diagnostically distinct patterns of energy state distributions

Nicholas Theis[1]

Jyotika Bahuguna[2]

Jonathan E. Rubin[3]

Joshua Cape[4]

Satish Iyengar[5]

Konasale M. Prasad[1,,6,7*]

[1]Department of Psychiatry, University of Pittsburgh School of Medicine, Pittsburgh, PA, USA

[2]Department of Neuroscience, Laboratoire de Neurosciences Cognitive et Adaptive, University of Strasbourg, France

[3]Department of Mathematics, University of Pittsburgh, PA, USA

[4]Department of Statistics, University of Wisconsin-Madison, WI, USA

[5]Department of Statistics, University of Pittsburgh, PA, USA

[6]Department of Bioengineering, Swanson School of Engineering, University of Pittsburgh, PA, USA

[7]Veterans Affairs Pittsburgh Healthcare System, Pittsburgh, PA, USA

***Corresponding author:**

3811 O'Hara Street, Pittsburgh, PA 15213, USA
KMP8@pitt.edu

Abstract

Objective

Existing neuroimaging studies of psychotic and mood disorders have reported regional brain activation differences (first-order properties) and alterations in functional connectivity based on pairwise correlations in activation (second-order properties). This study used a generalized Ising model, also called a pairwise maximum entropy model (MEM), to integrate first- and second-order properties to provide a comprehensive picture of BOLD patterns and a system-wide summary measure called energy. This study examines the usefulness of individual level MEMs, attempts to identify image-derived counterparts of the model, and explores potential applications to psychiatry.

Method

MEMs are fit to resting state fMRI data of each individual of a sample of 132 participants consisting of schizophrenia/schizoaffective disorder, bipolar disorder, and major depression, and a demographically matched 132 participants without these diagnoses from the UK Biobank to examine the default mode network (DMN).

Results

The model explained observed brain state occurrence probabilities well across all participants, and model parameters were highly correlated to image-derived parameters for all groups. Within clinical groups, schizophrenia/schizoaffective disorder and bipolar disorder patients showed significant differences in averaged energy distribution compared to controls for all sub-systems of the DMN except for depression, where differences in the energy distributions were only detected in the DMN of the regions from the right hemisphere.

Conclusions:

Subject-specific Ising modeling may offer an improved measure of biological functional correlates relative to traditional approaches. The observation of distinct patterns of energy distribution among the three clinical groups compared to controls suggests relative diagnostic specificity and potential for clinical translation.

Key words: Transdiagnostic approach; Generalized Ising model; Schizophrenia; Bipolar disorder; Major depression; Computational psychiatry; Network neuroscience

Introduction

Some elements of brain physiology can be described with a generalized Ising model (1-3), which expresses the probability that the system will be in any observable state according to a network of interacting brain regions (second-order properties) and of regional activations, often stimulus-evoked (first-order properties). Verisimilitude at the level of individual fMRI is apparent but not fully understood. Multifunctional cortical areas, subcortical nuclei, and their complex connectivity engender whole-brain dynamics (4, 5), driving metabolic changes to the blood oxygenation level-dependent (BOLD) signal (6). Temporal snapshots of this time-evolving system at multiple scales can be considered states in the same sense used in the Ising model, though these states are binary simplifications of the full underlying biological activity. Several previous studies on healthy individuals have shown that concatenated functional magnetic resonance imaging (fMRI) state occurrence patterns across individuals can be predicted using an Ising model (7-10), but only a few (11-13) have attempted to interpret the parameters of the model biologically or have applied it to psychiatric disorders (14).

The physiological relevance of the model is important to obtaining a more fine-grained understanding of the changes to brain connectivity associated with major psychiatric disorders such as schizophrenia, bipolar disorder, and major depression (15). Previous studies have concluded that the interaction matrix of the Ising model provides a more accurate measure of the underlying biology than traditional Pearson's correlation-based functional connectivity (FC), and that the two are similar (11, 13). However, most existing studies of the Ising model have used concatenated data across multiple participants to produce a single, group-level model. This presents a barrier to clinical use, where findings should be individually applicable avoiding ecological fallacy of using group level means to individual participants. This barrier is attributed to the need for many functional volumes to fit systems of even moderate size. For example, in a system of 10 regions of interest, if unequal state probabilities are expected, then the rarest states may be undetectable unless many more state observations are made than possible unique states, which is 1,024, and larger than the number of volumes acquired in the typical fMRI (16). The number of possible unique states in a system where regional activity is binary ("on" or "off"), is given by 2^N, where N is the number of regions. Faster (with shorter repetition time, TR) or longer imaging sequences and algorithmic improvements are necessary to make individual modeling realistic.

Fortunately, recent developments have shown it is possible to achieve individual level Ising model fitting (13, 17), which offers great clinical potential for psychiatry. In this study, we focus on the development of image-derived coefficients that can help distinguish apparently divergent pathologies underlying different disorders. Potential clinical applications ascribed to functional connectivity (18, 19) could be tested more rigorously in specific systems with this model, including theories about unbalanced connection strengths. We consider examined the regions included in the default mode network (DMN) in a transdiagnostic sample (N=132) and demographically matched controls (N=132) from the UK Biobank (20). The multimodal Glasser cortical parcellation was used to identify DMN regions (21) using a published data (22).

Alterations in DMN connectivity during resting state have long been associated with schizophrenia, depression, and other mood disorders (23-27). Our hypotheses were that 1) the models will fit different combination of regions from the DMN parcels selected from the Glasser atlas in all individuals, 2) the parameters of the Ising model determined by the MEM method will correspond to measures derived from traditional FC, and 3) state energies given by the model, which are inversely

related to state probabilities, will differ by each diagnostic group compared to controls. To test the third hypothesis, individual participants' averaged state-level energy values from each clinical group and the control group were compared.

Methods

The generalized Ising Model and the pairwise Maximum Entropy Model

The generalized Ising model is often used synonymously with the pairwise maximum entropy model (MEM) (28). The model is "generalized" in the sense that all node-pairs interact directly, whereas the originally proposed model is more limited (29, 30). MEM is pairwise because it considers up to the second order interaction (31). The model describes a system where the probabilities of occurrence of nodal binary on/off configurations (called states) are determined by the energetic interactions of the elements of the system in a network responding to an external field (32). According to the model, states for any subset of brain regions-of-interest will exhibit an energy given by the generalized Ising equation:

$$E(V_k) = -\sum_{i=1}^{N} h_i \sigma_i(V_k) - (1/2) \sum_{i=1}^{N} \sum_{j=1, j \neq i}^{N} J_{ij} \sigma_i(V_k) \sigma_j(V_k) \qquad (1)$$

In equation (1), the term energy, E, is defined for each brain state, V_k. The size of the system is N, which is the number of nodes (parcels) on which data is collected. The states themselves, σ_i, are binary, such that each $\sigma_i \in \{0,1\}$. For a given state number, k, the state V_k is a collection of N binary values representing binarized BOLD intensity at the imaged brain regions. The number of unique system states is given by the expression, 2^N. The energy of a given state, $E(V_k)$, is defined as the sum of first-order activation terms and half the sum of all second order co-activations (8). Each term h_i is the importance of the activation of the ith node, in the sense that certain nodes may have a greater influence over system dynamics than others and the vector h is also sometimes described as the external field. Each term J_{ij} encodes the relative importance of the co-activation of a pair of regions. J is symmetric using the implementation of MEM considered here, and the factor ½ in equation (1) compensates for double-counting.

The energy term, E, can be thought of as an abstract form of potential energy although with no absolute value or physical units. Instead, the energy of a given state is also related to the negative log probability of that state, $P(V_k)$, according to the Boltzmann distribution:

$$P(V_k) = \exp(-E(V_k)) / \sum_{i=1}^{2^N} \exp(-E(V_i)). \qquad (2)$$

Using a computational approach to map from probabilities, $P(V_k)$, computed from empirical observation to unknown Ising model parameters, J and h, is called inverse Ising inference. Implementations of this process, as well as equations and related Matlab, R, and python code can be found on GitHub (https://github.com/theisn/IsingModel_fMRI).

Data Source

Imaging data was sourced from the UK Biobank (www.ukbiobank.ac.uk), a biomedical database containing lifestyle and health data on more than 500,000 participants (20), including MRI data for some participants (33). The following UK Biobank data fields were used to obtain psychiatric disorders diagnosed according to the International Classification of Disease, 10th edition: data field 130874 Schizophrenia (F20); 130884 Schizoaffective disorder (F25); 130890 Manic Episode (F30); 130892 Bipolar Affective Disorder (F31); and 130896 Recurrent Depressive Disorder (F33) who were combined into three groups, namely schizophrenia/schizoaffective disorder (n=17), bipolar disorder (n=40) and major depressive disorder (n=75) (Total N=132).

To identify healthy controls matched for age and sex in the UK Biobank to match to each ICD disorder-diagnosed group, the above fields were excluded as well as the data field 20461, "age when first had unusual or psychotic experience", which indicates lifetime unusual and psychotic experiences (UPE). Using this method, we included 132 psychiatrically healthy participants.

Image Acquisition and Processing

Image acquisition parameters in the UK Biobank have been previously published (34). The UK Biobank is a multi-site study where all sites used identical Siemens Skyra 3T scanners with standard Siemens 32-channel receiving coils. T_1w images were acquired with a 3D MPRAGE sequence, 1mm isotropic voxels. For fMRI, a gradient echo-EPI sequence was used with x8 multi-slice acceleration, 2.4mm isotropic voxels, and a repetition time (TR) of 0.735 seconds for 490 timepoints.

The UK Biobank images were internally quality controlled and preprocessed (34). For fMRI, preprocessing steps included motion correction with MCFLIRT (35), grand-mean intensity normalization for each entire 4D acquisition, high-pass temporal filtering, EPI unwarping, gradient distortion correction, and ICA+FIX artifact removal (36, 37).

Additional image processing was performed using FSL and Freesurfer on the Pittsburgh Supercomputing Center's Bridges-2 system (38). These steps included Human Connectome Project (HCP) atlas parcellation (21) using the Neurolab (39) approach where an fs_average version of the human connectome project multi-modal atlas parcellation (40) was used to register the atlas to the individual result of FreeSurfer's "recon-all" function (Fischl 2012). Image co-registration of atlas parcellations to the fMRI was performed with FSL (35). MATLAB was used for voxel-wise averaging to generate nodal timeseries for each HCP parcel.

Region Selection

The DMN consists of 17 regions per hemisphere according to the Glasser atlas (22), namely, 10r, 31a, 31pd, 31pv, a24, d23ab, IP1, p32, POS1, POS2, RSC, PFm, PGi, PGs, s32, TPOJ3, and v23ab. A system of 34 nodes is far beyond practical size for the MEM. We selected anatomically diverse nodes to create three subsets of size $\leq$9 regions for the model, namely a bilateral system consisting of 4 regions from each hemisphere, and two mirrored unilateral models. Specifically, for the bilateral system, we selected POS1, p32m aTPOJ3, and PGi from each hemisphere because these regions were different sections on the HCP.

For the unilateral systems, when multiple nodes represented subdivisions of the same anatomical structure such as 31a, 31pd, 31pv and d23ab which represent the posterior cingulate gyrus, we included 31pv and d23ab within each hemisphere. For the anterior cingulate we included S32, 10r and a24. Other regions that were included were IP1 (area intraparietal), RSC (retrosplenial cortex), PFm (inferior parietal cortex), TPOJ3 (temporoparietal junction). Thus, for each unilateral model the nodes were: 10r, 31pv, a24, d23ab, IP1, S32, RSC, PFm, and TPOJ3.

Functional Connectivity

For each system, the FC was calculated as the Pearson's correlation (*r*) between node-pairs and encoded using an adjacency matrix. FC is hypothesized to correlate with co-activation parameters of the model, *J* and *h* is interpretable as a vector of activation levels in the absence of an external field, or "firing rate" (Gu et al. 2018). However, in our implementation, each nodal time series is independently z-scored (see next section), so all nodes have mean activation levels of about 0.5. Instead, we introduced the following formula to compute intrinsically from FC to compare with *h*:

$$h_i = \text{-strength}(FC_i) \qquad (3)$$

where the strength() function is the graph theoretical nodal strength and *i* is the node index (41). This is equivalent to either the *i*th row sum or column sum of the adjacency matrix when FC is symmetric, which is the case here.

Observed Binary States (B)

After regional voxel averaging, fMRI signals are *z*-scored per subject, per node. *Z*-scoring of fMRI data is widely used in fMRI studies (42, 43) since the units of the original BOLD signal are arbitrary and have unknown baseline offsets. Next, the global signal across all nodes is subtracted out, which is substantially similar to global signal normalization (44)(. This step has little visual effect on the data (**Figure 1**).

To generate a binary matrix B representing brain states from regional time series data, a threshold of zero is applied to each data point. The mean activation level is by definition zero after z-scoring, resulting in a B matrix with 50% "on" states and 50% "off" states (i.e., 50% of entries in each row of matrix B are 1 and 50% are 0). This threshold, zero, has previously been determined to be the most optimal threshold choice in terms of fit of MEM to empirical observations (14).

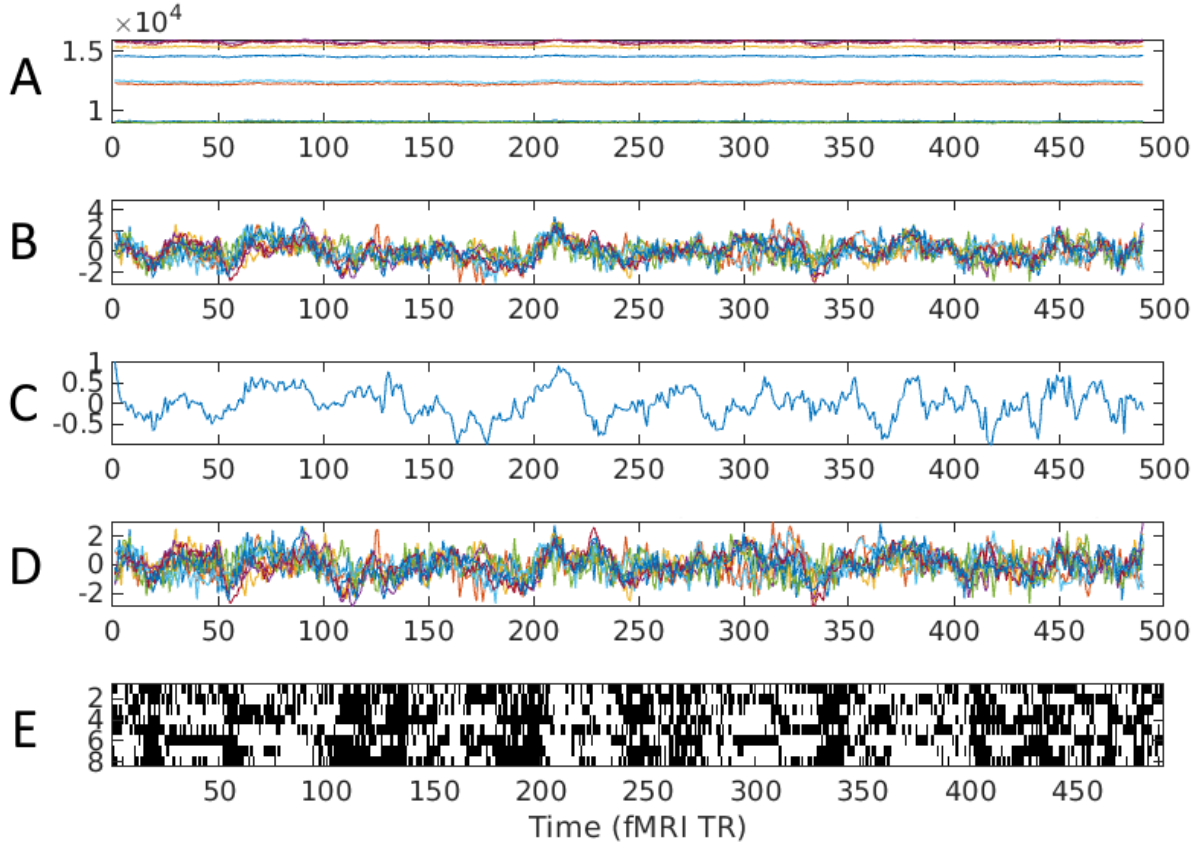

Figure 1. Post-processing and Binarization. All x-axes show time in fMRI volumes, Repetition Time (TR); each TR is 0.735 seconds. **A)** The preprocessed BOLD signals in amplitude of arbitrary units for a single subject for the 8 bilateral nodes: POS1, p32m aTPOJ3, and PGi in both hemispheres. **B)** The z-scored amplitude nodal time-series has an average centered at zero and is scaled to a standard deviation of one. **C)** The global signal across all z-scored nodes in the entire brain is shown, followed by **D)** the z-scores after subtracting this value. Finally, **E)** the time series are binarized at the threshold of zero, where the y-axis is now node index, rather than amplitude. White cells indicate the "on" nodes at the given time, indicating that the value in **D** for that node was greater than zero, while black cells indicate "off" nodes.

Maximum Likelihood Estimation (MLE) of the MEM

The maximum-entropy estimate was first proposed by Edwin Jaynes to find "maximally noncommittal" solutions to statistical inference in systems with missing information (45). The principle of maximum entropy provides a robust optimization criterion, but specific optimal parameters for the MEM must be obtained computationally. One approach to finding the coefficients of the MEM is applying gradient descent to perform MLE, based on the log-likelihood function, given the set of observed brain states (13, 17).

Statistics Model fits are evaluated after convergence by correlating the theoretical probability given by calculating $P(V_k)$ for each state in V_k using equations (1) and (2) to the corresponding observed probability for each subject. The strength of this correlation indicates the validity of the model parameters, J and h. The relationship of J to the FC and h to the negative strengths of the FC from equation (3) were further tested using Pearson's correlation. Finally, the energy profiles, $E(V_k)$, for each state V_k are

averaged across all subjects in each clinical group and across controls. The resulting histograms are compared using a two-sample Kolmogorov-Smirnov test for differences in distributions.

Results

Demographics

A demographic breakdown by diagnosis is given in **(Table 1).**

	Schizophrenia/ Schizoaffective	SZ/SA Controls	Bipolar/ Manic	B/M Controls	Depression	Depression Controls
Sample Size	17	17	40	40	75	75
Age	52.6 (±6.5)	52.6 (±6.5)	53.4(±7.3)	53.4(±7.3)	53.6(±7.4)	53.6(±7.4)
% Female	70.6%	70.6%	55.0%	55.0%	72.0%	72.0%

Table 1. Demographics. UK Biobank participant Demographics. Schizophrenia (SZ) and schizoaffective (SA) are considered together. The bipolar disorder (B) and the manic (M) participants without SZ/SA status are considered together. The depression participants without SZ/SA nor B/M are considered together. Age is reported in years.

The demographic data (Table 1) shows that the groups were matched for age and sex with no statistically significant differences among the groups.

Model Fit

Individual level MLE fits of the MEM to the empirical probabilities of state occurrence were statistically significant in all subjects and subsystems of nodes considered, for all the clinical groups and controls (**Figure 2**). The majority of correlations exceeded 0.9 (average r=0.91 (±0.064), p<1e-62). A small fraction of subjects had lower correlations of 0.5 < r < 0.9. A small fraction of subjects showed correlation strengths of 0.5 < r < 0.9, but all were significant correlations (p<0.1e-23). In contrast, using FC to determine the values of J and equation (3) for h resulted in lower correlations between observed and predicted states (average r<0.7) in all cases (**Supplemental Figure S1**). Group differences were not found in the model fits.

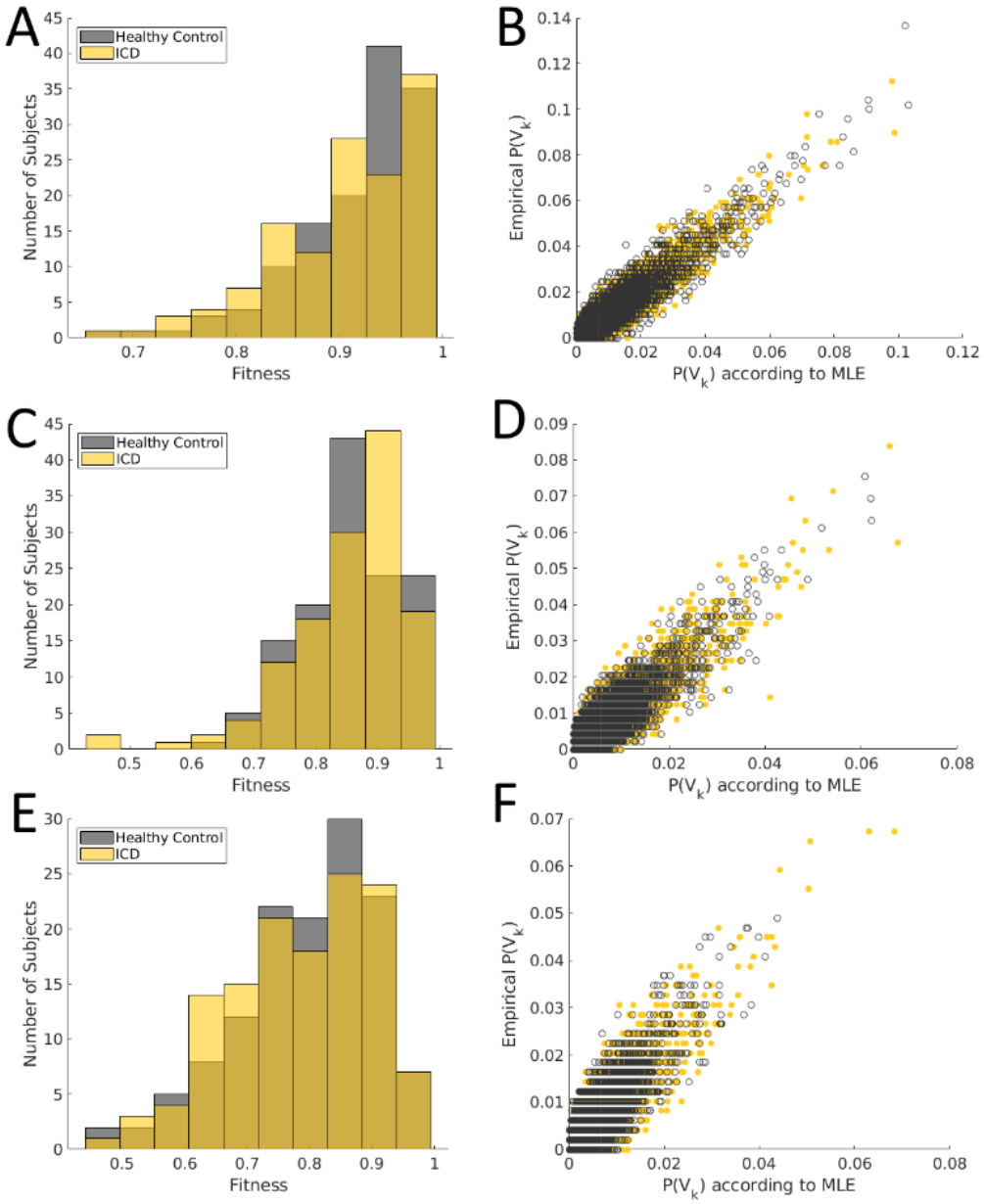

Figure 2. Model Fits. Bilateral: top row**. Left Hemisphere:** middle row. **Right Hemisphere:** bottom row. **A) bilateral:** two histograms, pooled ICD (N=132) in yellow and pooled HC (N=132) in black are compared. Fitness (x-axis) is the correlation between predicted $P(V_k)$ according to the model and observed $P(V_k)$ per individual. **B) bilateral:** all unique possible states are shown for all subjects according to their probability predicted from the MEM (x-axis) versus their empirical observed probability (y-axis). Black circles represent data from controls, yellow points represent data from the ICD group. **C) left hemisphere:** fit histograms for pooled ICD (yellow) and pooled HC (black) are compared. **D) left hemisphere:** all unique possible states are shown for all subjects according to their predicted probability (x-axis) versus their observed probability (y-axis). Black circles represent data from controls, yellow points represent data from the ICD group. **E) right hemisphere:** fit histograms for pooled ICD (yellow) and pooled HC (black) are compared. **F) right hemisphere:** all unique possible states are shown for all subjects according to their predicted probability (x-axis) versus their observed probability (y-axis). Black circles represent data from controls, yellow points represent data from the ICD group.

Similarity of Ising Model Parameters to FC

There were significant correlations between Ising model parameters and image-derived coefficients in all individuals and systems (**Figure 3**). However, subjects with psychiatric disorders as a group and controls did not show significant differences. The relationship between *J* and FC appears sigmoidal, based on the fact that FC is bounded by 1, with a linear relation outside of the saturating part of the sigmoid. The correlation between *h* and the image-derived coefficients associated with *h* at the individual level, computed from equation (3), was stronger than the *J*-FC correlation in most subjects.

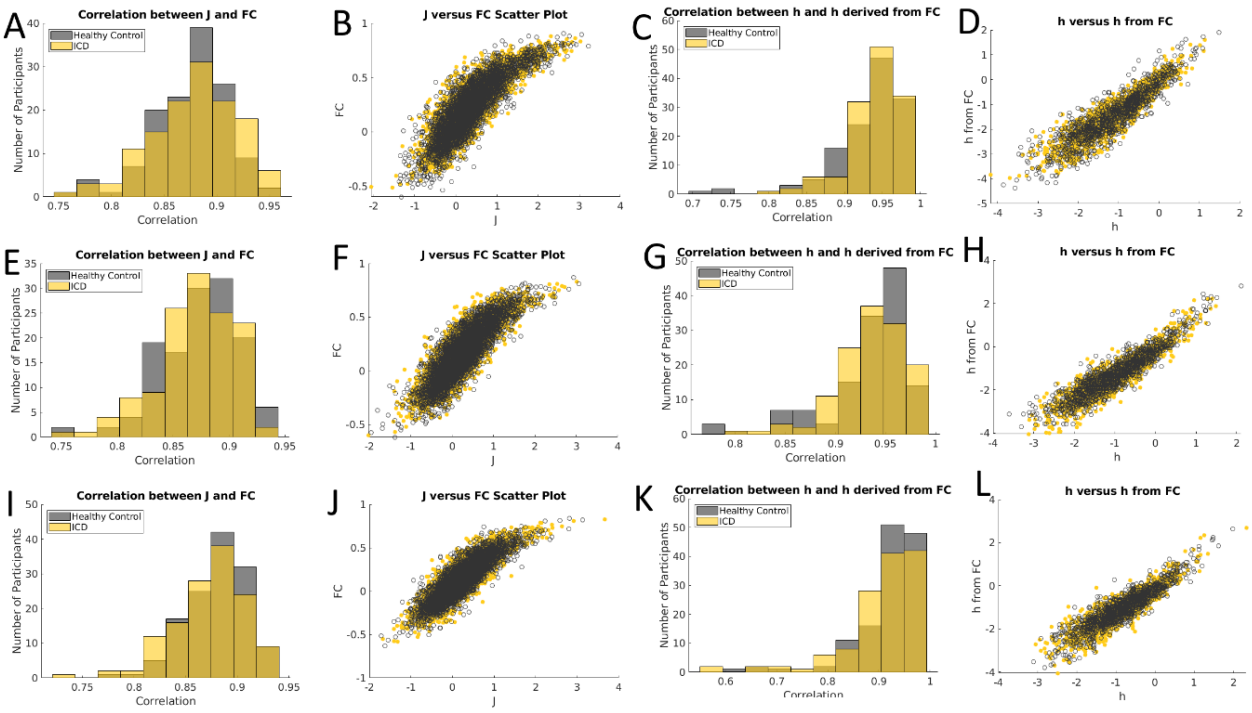

Figure 3. Comparison of MLE- and image-derived MEM coefficients. Bilateral: top row**. Left Hemisphere:** middle row. **Right Hemisphere:** bottom row. **A) bilateral:** two histograms, pooled ICD (N=132) in yellow and pooled HC (N=132) in black are compared. Each histogram represents the population-wide distribution of correlations between the second-order *J* parameter (x-axis) compared to edge weights of the FC (y-axis). **B) bilateral:** scatter plots of all subjects and all parameter values showing a strong relationship between *J* and FC; black circles are HC, yellow points are ICD **C) bilateral:** histograms for group-wise distributions of correlations between h from the MEM and the image-derived coefficients in equation (3). **D) bilateral:** individual scatter plots for all participants between h (x-axis) and the image-derived coefficients (y-axis). **E) left hemisphere:** group-wise population histograms of *J*-to-FC similarity. **F) left hemisphere:** all individual-level scatter plot data for corresponding parameters in *J* (x-axis), and FC (y-axis). **G) left hemisphere:** histograms for group-wise distributions of correlations between h from the MEM and the image-derived coefficients in equation (3). **H) left hemisphere:** individual scatter plots for all participants between *h* (x-axis) and the image-derived coefficients (y-axis). **I) right hemisphere:** group-wise population histograms of *J*-to-FC similarity. **J) right hemisphere:** all individual-level scatter plot data for corresponding parameters in *J* (x-axis), and FC (y-axis). **K) right hemisphere:** histograms for group-wise distributions of correlations between *h* from the MEM and the image-derived coefficients in equation (3). **H) right hemisphere:** individual scatter plots for all participants between h (x-axis) and the image-derived coefficients (y-axis).

Energy Profiles by Clinical Group

In the bilateral DMN system, the energy distributions across system states forthe depression group and their demographically matched controls did not differ (KS=0.090, p=0.241), but both the bipolar disorder (KS=0.406, p=3.38e-19) and the SZ/SZA energy distributions (KS=0.301, p=1.025e-10) were significantly different from their controls (**Figure 4A-C**). In the left hemisphere DMN system, the group-wide average energy profiles followed the same trends as the bilateral case for the SZ/SZA, bipolar disorder and depression groups (**Figures 4D-F**). The right hemisphere DMN system followed a similar trend as the bilateral system with bipolar disorder (KS=0.315, p=9.20e-23) and SZ/SZA (KS=0.404, p=2.38e-37) having significantly different distributions; unlike the other DMN systems, for this one, the depression group also was found to have a significantly different energy distribution from the demographically matched HC (KS=0.127, p=4.57e-04) (**Figure 4G-I**).

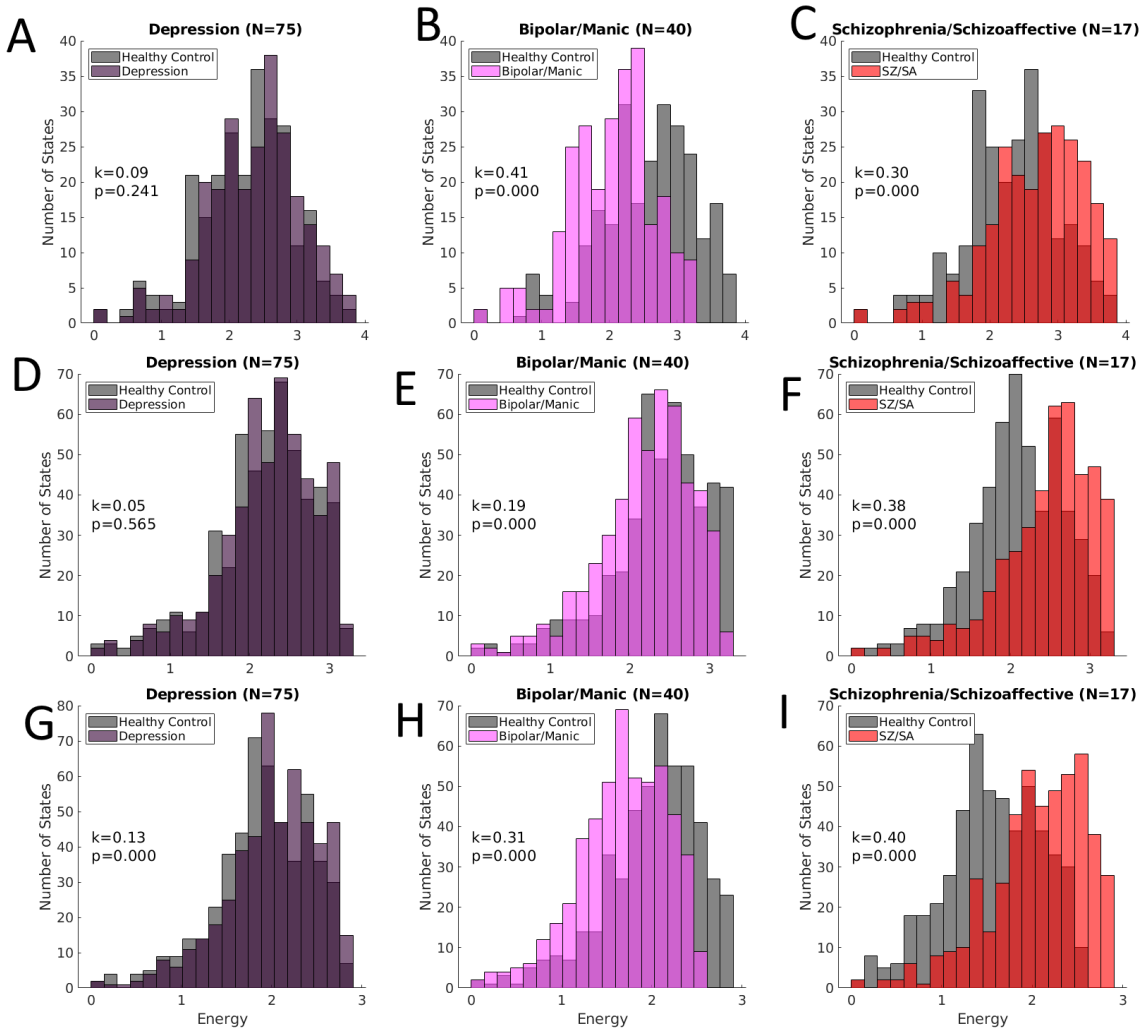

Figure 4. Energy Profiles by Clinical Group. Bilateral: top row**. Left Hemisphere:** middle row. **Right Hemisphere:** bottom row. Statistics reported in plots are KS statistics and associated p-value. **A) bilateral:** The group-wise average energy profile of depression compared to controls. **B) bilateral:** bipolar/manic compared to controls. **C) bilateral:** SZ/SA compared to controls. **D) left hemisphere:** depression compared to controls. **E) left hemisphere:** bipolar/manic compared to controls. **F) left hemisphere:** SZ/SA compared to controls. **G) right hemisphere:** depression compared to controls. **H) right hemisphere:** bipolar/manic compared to controls. **I) right hemisphere:** SZ/SA compared to controls.

Discussion

Summary of Findings

The MLE algorithm for inferring Ising model coefficients converged across all node collections considered in every subject, as anticipated (13, 17). The correlation between the predicted and observed $P(V_k)$ distributions at the individual subject level was high (**Figures 2**) and exceeded the correlation derived directly from FC, suggesting that the Ising model provides a good representation of how often the states of the system arise. Moreover, the image-derived coefficients from FC correlate with the model parameters, *h* and *J* (**Figures 3**), suggesting that the MEM could be considered as an alternative estimate of biological connectivity that gives an especially useful representation of overall brain states. The clinical findings (**Figure 4**) suggest that DMN abnormalities of connectivity and intrinsic activity may be diagnostically specific and detectable using the Ising model framework.

Interpretations of the Ising Model

Interacting brain regions can be considered as active or inactive using a scientifically justified threshold, or similarly in more complex representations, can have firing rates or phases (3). Since the fMRI signal has no physical units, is not calibrated (46), and represents blood oxygenation level differences, blood flow, and the volume of the region being perfused, the relevance of the neural Ising model hypothesis to single-participant level subsystems of anatomically informed brain atlas regions (21, 22) in resting state fMRI is not well characterized. Yet there is a strong case that neural activity, specifically local field potentials (LFP) and calcium signaling are hemodynamically coupled (6, 47, 48), so it is plausible that some fMRI data have Ising-like properties. This observation leads to the hypothesis that some image-derived coefficients may relate to the Ising model parameters, *J* and *h*. Attempts to directly use image-derived coefficients, in particular the modularity matrix of the diffusion MRI derived structural connectome (SC), as a starting point for a forward solution (Gu et al. 2018), where *J* and *h* are computed directly and thus not solved for using the MEM approach have not reported the relationship between actual brain state occurrence frequencies and model predictions, focusing instead on firing rates, where model predictions have poor correlations (r=0.18) at low thresholds and moderate correlations at high thresholds (r=0.31). Another study (Watanabe et al. 2013) proposed that the *J* matrix from the pairwise MEM (**Equation 1**) would explain the system interaction better than traditional FC, while hypothesizing correctly that this parameter has substantial similarity to FC. That study indeed reported that the *J* matrix MEM solution corresponds very closely to the FC and that stronger connections in *J* are very likely to co-occur with diffusion streamline connections in the SC (11). Other recent studies have examined the relationship between *J* and the SC in more detail (13, 31). Though related to each other, the SC, representing axonal diffusion streamlines, and the FC, representing statistical co-activity of BOLD signal time-series, are in many ways different (49). For instance, the FC represents polysynaptic connections, whereas the SC represents monosynaptic connections. It is therefore unlikely that SC can be a direct substitute for *J*. Substituting FC directly for *J* and equation (3) for *h* is also problematic, as it results in non-significant model fits between the observed state probabilities and the predicted state probabilities (**Supplemental Figure S1**).

We identified only several existing attempts in the literature to find image-derived coefficients related to the first order activation parameter, *h* (13). In some contexts, particularly its native context of

physics, the *h* parameter in the Ising model is described as the "external field". While this has a more straightforward interpretation in magnetism, it could be considered equivalent to the notion of receptive field (50) in neuroscience. This is not to suggest that there is any basis for a claim relating the BOLD signal to functional localization or neural computation directly, just that the *h* parameter in the Ising model may be theoretically related to the external environment. Since this study used resting state fMRI there is not likely to be an external stimulus source besides the fixation cross and the scanner noise. In either case (resting or task fMRI), we suggest equation (3) as the starting point for an image-derived representation of *h*.

Limitations to the Ising Model and the MEM

All Ising model studies are limited by the exponential growth of the MEM in terms of number of unknown variables as a function of the number of nodes included in the model. While individual level modeling raises the possibility of discovering a forward, image-derived solution, large systems will yield vanishingly small probabilities for individual brain states, fundamentally limiting Ising model application to relatively smaller systems. Additionally, while more specific to fMRI than the Ising model itself, recent studies have shown that findings reported in traditional second-order statistical FC studies are not very reliable (51) nor are first-order brain-wide association findings (52). While the Ising model provides an improved estimate of FC and can be used to estimate first order nodal activity, it is not clear to what extent this model helps overcome the inter-study reliability issues associated with fMRI studies.

Conclusions and Future Directions

The findings presented here demonstrate that individual subject fMRI scans are amenable to Ising model fitting techniques. Individual level fitting has only recently been made possible, and to our knowledge this is the first application of the method to psychiatric neuroimaging. While the clinical findings would need to be replicated in independent samples, our results suggest that it may be possible to characterize biomarkers using energy. In SZ/SZA, DMN states were found to be of higher energy than corresponding states in controls, and thus less structured. The bipolar group had overall lower energy states than controls suggesting the DMN may have a larger number of stable alternative resting states. For the depression group there may be abnormal DMN functional lateralization, but overall may not be significantly different from controls.

The translational goals of traditional FC studies (53), such as treatment response (54), therapeutic targeting, biomarker identification (55) and pathophysiological implications can be tested in the generalized Ising model framework which provides an improved estimate of the underlying biological connectivity. The MEM paradigm provides a principled, unified solution to first and second order model parameters and a theoretical system of interaction that yields testable state probability predictions from these parameters. Future research should focus on clinical translatability of this model and look beyond resting state fMRI to examine task-associated brain networks in disease-implicated cognition.

Data availability

The data is available through NIMH data repository.

Funding Sources

Funding was provided by NIMH grant numbers: R01MH115026 and R01MH112584 (KMP).

Conflicts of Interest:

All authors declare no conflicts of interest associated with this work.

Author Contributions

NT conceptualized the study analysis, performed analysis and drafted the manuscript; JB helped with MEM implementation, performed analysis and participated in editing the manuscript; JR supervised the analysis and participated in drafting and editing manuscript; JC and SI participated in the discussion of the analysis and edited the manuscript; KP managed the data procurement for the study, conceptualized the study design, supervised the analysis, and participated in drafting and editing manuscript.

REFERENCES

1. Amit DJ, Gutfreund H, Sompolinsky H. Spin-glass models of neural networks. Phys Rev A Gen Phys. 1985;32:1007-1018.
2. Fraiman D, Balenzuela P, Foss J, Chialvo DR. Ising-like dynamics in large-scale functional brain networks. Phys Rev E Stat Nonlin Soft Matter Phys. 2009;79:061922.
3. Hopfield JJ. Neural networks and physical systems with emergent collective computational abilities. Proceedings of the National Academy of Sciences of the United States of America. 1982;79:2554-2558.
4. Chialvo DR. Emergent complex neural dynamics. Nature Physics. 2010;6:744-750.
5. Gilson M, Moreno-Bote R, Ponce-Alvarez A, Ritter P, Deco G. Estimation of Directed Effective Connectivity from fMRI Functional Connectivity Hints at Asymmetries of Cortical Connectome. PLoS Comput Biol. 2016;12:e1004762.
6. Drew PJ. Vascular and neural basis of the BOLD signal. Curr Opin Neurobiol. 2019;58:61-69.
7. Das TK, Abeyasinghe PM, Crone JS, Sosnowski A, Laureys S, Owen AM, Soddu A. Highlighting the structure-function relationship of the brain with the Ising model and graph theory. Biomed Res Int. 2014;2014:237898.
8. Yeh FC, Tang AN, Hobbs JP, Hottowy P, Dabrowski W, Sher A, Litke A, Beggs JM. Maximum Entropy Approaches to Living Neural Networks. Entropy. 2010;12:89-106.
9. Watanabe T, Kan S, Koike T, Misaki M, Konishi S, Miyauchi S, Miyahsita Y, Masuda N. Network-dependent modulation of brain activity during sleep. NeuroImage. 2014;98:1-10.
10. Ezaki T, Watanabe T, Ohzeki M, Masuda N. Energy landscape analysis of neuroimaging data. Philos Trans A Math Phys Eng Sci. 2017;375:20160287.
11. Watanabe T, Hirose S, Wada H, Imai Y, Machida T, Shirouzu I, Konishi S, Miyashita Y, Masuda N. A pairwise maximum entropy model accurately describes resting-state human brain networks. Nat Commun. 2013;4:1370.
12. Gu S, Cieslak M, Baird B, Muldoon SF, Grafton ST, Pasqualetti F, Bassett DS. The Energy Landscape of Neurophysiological Activity Implicit in Brain Network Structure. Sci Rep. 2018;8:2507.
13. Kang J, Jeong SO, Pae C, Park HJ. Bayesian estimation of maximum entropy model for individualized energy landscape analysis of brain state dynamics. Human brain mapping. 2021;42:3411-3428.
14. Theis N, Bahuguna J, Rubin J, Muldoon B, Prasad KM. Energy in functional brain states correlates with cognition in adolescent schizophrenia and healthy persons. bioRxiv. 2023.
15. Sharma A, Wolf DH, Ciric R, Kable JW, Moore TM, Vandekar SN, Katchmar N, Daldal A, Ruparel K, Davatzikos C, Elliott MA, Calkins ME, Shinohara RT, Bassett DS, Satterthwaite TD. Common Dimensional Reward Deficits Across Mood and Psychotic Disorders: A Connectome-Wide Association Study. The American journal of psychiatry. 2017;174:657-666.
16. Birn RM, Molloy EK, Patriat R, Parker T, Meier TB, Kirk GR, Nair VA, Meyerand ME, Prabhakaran V. The effect of scan length on the reliability of resting-state fMRI connectivity estimates. NeuroImage. 2013;83:550-558.
17. Jeong SO, Kang J, Pae C, Eo J, Park SM, Son J, Park HJ. Empirical Bayes estimation of pairwise maximum entropy model for nonlinear brain state dynamics. NeuroImage. 2021;244:118618.
18. Ball TM, Goldstein-Piekarski AN, Gatt JM, Williams LM. Quantifying person-level brain network functioning to facilitate clinical translation. Translational psychiatry. 2017;7:e1248.
19. Gratton C, Kraus BT, Greene DJ, Gordon EM, Laumann TO, Nelson SM, Dosenbach NUF, Petersen SE. Defining Individual-Specific Functional Neuroanatomy for Precision Psychiatry. Biological psychiatry. 2020;88:28-39.
20. Littlejohns TJ, Holliday J, Gibson LM, Garratt S, Oesingmann N, Alfaro-Almagro F, Bell JD, Boultwood C, Collins R, Conroy MC, Crabtree N, Doherty N, Frangi AF, Harvey NC, Leeson P, Miller KL, Neubauer S, Petersen SE, Sellors J, Sheard S, Smith SM, Sudlow CLM, Matthews PM, Allen NE. The UK Biobank

imaging enhancement of 100,000 participants: rationale, data collection, management and future directions. Nat Commun. 2020;11:2624.
21. Glasser MF, Coalson TS, Robinson EC, Hacker CD, Harwell J, Yacoub E, Ugurbil K, Andersson J, Beckmann CF, Jenkinson M, Smith SM, Van Essen DC. A multi-modal parcellation of human cerebral cortex. Nature. 2016;536:171-178.
22. Sandhu Z, Tanglay O, Young IM, Briggs RG, Bai MY, Larsen ML, Conner AK, Dhanaraj V, Lin YH, Hormovas J, Fonseka RD, Glenn CA, Sughrue ME. Parcellation-based anatomic modeling of the default mode network. Brain Behav. 2021;11:e01976.
23. Garrity AG, Pearlson GD, McKiernan K, Lloyd D, Kiehl KA, Calhoun VD. Aberrant "default mode" functional connectivity in schizophrenia. The American journal of psychiatry. 2007;164:450-457.
24. Broyd SJ, Demanuele C, Debener S, Helps SK, James CJ, Sonuga-Barke EJ. Default-mode brain dysfunction in mental disorders: a systematic review. Neurosci Biobehav Rev. 2009;33:279-296.
25. Whitfield-Gabrieli S, Ford JM. Default mode network activity and connectivity in psychopathology. Annu Rev Clin Psychol. 2012;8:49-76.
26. Doucet GE, Bassett DS, Yao N, Glahn DC, Frangou S. The Role of Intrinsic Brain Functional Connectivity in Vulnerability and Resilience to Bipolar Disorder. The American journal of psychiatry. 2017;174:1214-1222.
27. Doucet GE, Janiri D, Howard R, O'Brien M, Andrews-Hanna JR, Frangou S. Transdiagnostic and disease-specific abnormalities in the default-mode network hubs in psychiatric disorders: A meta-analysis of resting-state functional imaging studies. European psychiatry : the journal of the Association of European Psychiatrists. 2020;63:e57.
28. Kloucek MB, Machon T, Kajimura S, Royall CP, Masuda N, Turci F. Biases in inverse Ising estimates of near-critical behavior. Phys Rev E. 2023;108:014109.
29. Ising E: Beitrag zur Theorie des Ferro- und Paramagnetismus. in Department of Physics, University of Hamburg; 1924.
30. Ising T, Folk R, Kenna R, Berche B, Holovatch Y. The Fate of Ernst Ising and the Fate of his Model. arXiv: History and Philosophy of Physics. 2017.
31. Ashourvan A, Shah P, Pines A, Gu S, Lynn CW, Bassett DS, Davis KA, Litt B. Pairwise maximum entropy model explains the role of white matter structure in shaping emergent co-activation states. Commun Biol. 2021;4:210.
32. Knuuttila T, Loettgers A. Magnets, Spins, and Neurons: The Dissemination of Model Templates across Disciplines. Monist. 2014;97:280-300.
33. Miller KL, Alfaro-Almagro F, Bangerter NK, Thomas DL, Yacoub E, Xu J, Bartsch AJ, Jbabdi S, Sotiropoulos SN, Andersson JL, Griffanti L, Douaud G, Okell TW, Weale P, Dragonu I, Garratt S, Hudson S, Collins R, Jenkinson M, Matthews PM, Smith SM. Multimodal population brain imaging in the UK Biobank prospective epidemiological study. Nature neuroscience. 2016;19:1523-1536.
34. Smith S, Alfaro-Almagro F, Miller K: UK Biobank Brain Imaging Documentation. Wellcome Centre for Integrative Neuroimaging (WIN-FMRIB), Oxford University on behalf of UK Biobank, http://www.ukbiobank.ac.uk; 2020.
35. Jenkinson M, Beckmann CF, Behrens TE, Woolrich MW, Smith SM. Fsl. NeuroImage. 2012;62:782-790.
36. Beckmann CF, Smith SM. Probabilistic independent component analysis for functional magnetic resonance imaging. IEEE transactions on medical imaging. 2004;23:137-152.
37. Salimi-Khorshidi G, Douaud G, Beckmann CF, Glasser MF, Griffanti L, Smith SM. Automatic denoising of functional MRI data: combining independent component analysis and hierarchical fusion of classifiers. NeuroImage. 2014;90:449-468.
38. Buitrago P, Nystrom N: Neocortex and Bridges-2: A High Performance AI+HPC Ecosystem for Science, Discovery, and Societal Good High Performance Computing; 2021. pp. 205-219.

39. Neurolab C: HCP-MMP1.0 volumetric (NIfTI) masks in native structural space. figshare2017. pp. Dataset.
40. Mills K: HCP-MMP1.0 projected on fsaverage. Edited by figshare2016.
41. Sporns O. Graph theory methods: applications in brain networks. Dialogues Clin Neurosci. 2018;20:111-121.
42. Cho JW, Korchmaros A, Vogelstein JT, Milham MP, Xu T. Impact of concatenating fMRI data on reliability for functional connectomics. NeuroImage. 2021;226:117549.
43. Jo Y, Faskowitz J, Esfahlani FZ, Sporns O, Betzel RF. Subject identification using edge-centric functional connectivity. NeuroImage. 2021;238:118204.
44. Liu TT, Nalci A, Falahpour M. The global signal in fMRI: Nuisance or Information? NeuroImage. 2017;150:213-229.
45. Jaynes ET. Information Theory and Statistical Mechanics. Physical Review. 1957;106:620-630.
46. Hoge RD. Calibrated FMRI. NeuroImage. 2012;62:930-937.
47. Logothetis NK. The ins and outs of fMRI signals. Nature neuroscience. 2007;10:1230-1232.
48. Hillman EM. Coupling mechanism and significance of the BOLD signal: a status report. Annu Rev Neurosci. 2014;37:161-181.
49. Suarez LE, Markello RD, Betzel RF, Misic B. Linking Structure and Function in Macroscale Brain Networks. Trends in cognitive sciences. 2020;24:302-315.
50. Spillmann L, Dresp-Langley B, Tseng CH. Beyond the classical receptive field: The effect of contextual stimuli. J Vis. 2015;15:7.
51. Noble S, Scheinost D, Constable RT. A decade of test-retest reliability of functional connectivity: A systematic review and meta-analysis. NeuroImage. 2019;203:116157.
52. Marek S, Tervo-Clemmens B, Calabro FJ, Montez DF, Kay BP, Hatoum AS, Donohue MR, Foran W, Miller RL, Hendrickson TJ, Malone SM, Kandala S, Feczko E, Miranda-Dominguez O, Graham AM, Earl EA, Perrone AJ, Cordova M, Doyle O, Moore LA, Conan GM, Uriarte J, Snider K, Lynch BJ, Wilgenbusch JC, Pengo T, Tam A, Chen J, Newbold DJ, Zheng A, Seider NA, Van AN, Metoki A, Chauvin RJ, Laumann TO, Greene DJ, Petersen SE, Garavan H, Thompson WK, Nichols TE, Yeo BTT, Barch DM, Luna B, Fair DA, Dosenbach NUF. Reproducible brain-wide association studies require thousands of individuals. Nature. 2022;603:654-660.
53. van den Heuvel MP, Hulshoff Pol HE. Exploring the brain network: a review on resting-state fMRI functional connectivity. Eur Neuropsychopharmacol. 2010;20:519-534.
54. Goff DC, Roffman J, Holt DJ. Another Step Toward the Prediction of Antipsychotic Treatment Response Using Functional Connectivity. The American journal of psychiatry. 2023;180:787-788.
55. Kraguljac NV, McDonald WM, Widge AS, Rodriguez CI, Tohen M, Nemeroff CB. Neuroimaging Biomarkers in Schizophrenia. The American journal of psychiatry. 2021;178:509-521.

Supplement

Substituting FC for *J* and equation (3) for *h* results in non-significant model fits (**Supplemental Figure S1**). Since the parameters in the Ising model, (**Equation 1**) are unknown and must be computed using the MEM, and because the computed parameters from the MEM correlate significantly with image-derived variables (**Figure 3**)**,** it is reasonable to assume that substituting the image-derived values for the MEM-derived values will also result in good fits, similar to those shown in (**Figure 2**)**.** This does not turn out to be the case. Image-derived parameters result in poor predictions of observed state occurrence probability.

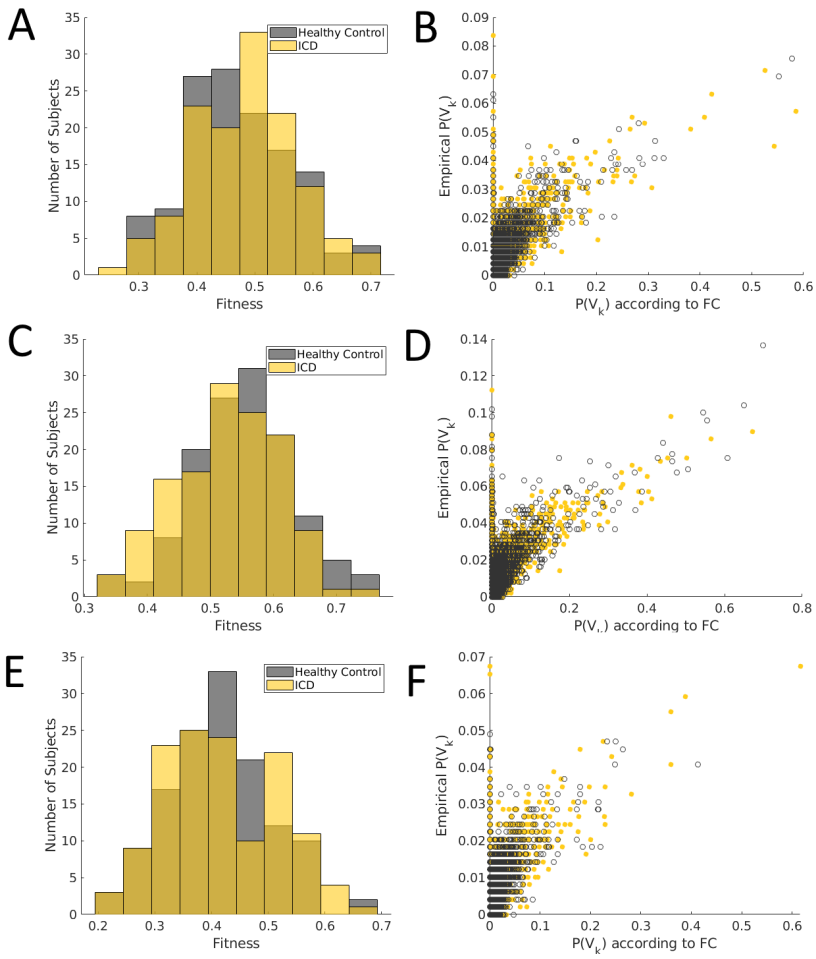

Supplemental Figure S1. Fits according to image-derived coefficients. Bilateral: top row**. Left Hemisphere:** middle row. **Right Hemisphere:** bottom row. **A) bilateral:** two histograms, pooled ICD (N=132) in yellow and pooled HC (N=132) in black are compared. Fit (x-axis) is the correlation between predicted $P(V_k)$ according to the image-derived variables and observed $P(V_k)$ per individual. **B) bilateral:** all unique possible states are shown for all subjects according to their predicted probability (x-axis) versus their observed probability (y-axis). Black circles represent data from controls, yellow points represent data from the ICD group. **C) left hemisphere:** fit histograms for pooled ICD (yellow) and pooled HC (black) are compared. **D) left hemisphere:** all unique possible states are shown for all subjects according to their predicted probability (x-axis) versus their observed probability (y-axis). Black circles represent data

from controls, yellow points represent data from the ICD group. **E) right hemisphere:** fit histograms for pooled ICD (yellow) and pooled HC (black) are compared. **F) right hemisphere:** all unique possible states are shown for all subjects according to their predicted probability (x-axis) versus their observed probability (y-axis). Black circles represent data from controls, yellow points represent data from the ICD group.